JACS
JOURNAL OF THE AMERICAN CHEMICAL SOCIETY
Communication
pubs.acs.org/JACS

Controlled Chemical Doping of Semiconductor Nanocrystals Using Redox Buffers

Jesse H. Engel,[†,‡,∥] Yogesh Surendranath,[†,§,∥] and A. Paul Alivisatos*[,†,‡]

[†]Department of Chemistry, University of California, Berkeley, California 94720, United States,
[‡]Materials Sciences Division, Lawrence Berkeley National Laboratory, Berkeley, California 947203, United States,
[§]Miller Institute for Basic Research in Science, University of California, Berkeley, California 94720, United States

Supporting Information

ABSTRACT: Semiconductor nanocrystal solids are attractive materials for active layers in next-generation optoelectronic devices; however, their efficient implementation has been impeded by the lack of precise control over dopant concentrations. Herein we demonstrate a chemical strategy for the controlled doping of nanocrystal solids under equilibrium conditions. Exposing lead selenide nanocrystal thin films to solutions containing varying proportions of decamethylferrocene and decamethylferrocenium incrementally and reversibly increased the carrier concentration in the solid by 2 orders of magnitude from their native values. This application of redox buffers for controlled doping provides a new method for the precise control of the majority carrier concentration in porous semiconductor thin films.

Semiconductor nanocrystal solids are a novel class of solution-processable, modular materials that have seen increasing use as active layers for next-generation optoelectronic devices.[1−3] These solids consist of macroscopic arrays of colloidally synthesized nanoparticles wherein the band gap and the electronic properties of the composite array can be tuned by varying the size[4] and surface chemistry[5] of the constitutive elements, respectively. The integration of these solids into functional devices requires control over the dopant density in the material. To this end, postsynthetic chemical treatments[6−9] have emerged as promising methods for controlling the free carrier concentrations in nanocrystal solids.

Chemical doping methods[6−9] reported to date have primarily relied on exergonic reactions in which stoichiometric or kinetic limitations are used to control the degree of doping instead of direct modulation of the Fermi level under equilibrium conditions. For these approaches, the final doping density and homogeneity within the nanocrystal film is a complex convolution of unknown reaction rates for charge transfer, surface coordination, and/or diffusion. Indeed, the precise mechanism of doping remains ill-defined in most cases,[10,11] making a kinetic description intractable at present. In contrast to chemical methods, thermodynamic control of doping has been achieved using electrochemical methods, which shift the Fermi level of the nanocrystal solid through reversible charge transfer from the electrode.[12−15] Fine control over the applied potential (±1 mV) allows the doping level to be set with precision. Despite this advantage, electrochemical doping methods require metallic back contacts and suffer from Ohmic potential losses across weakly conductive films, limiting available device architectures.

Herein we combine the precision afforded by electrochemical doping methods with the simplicity and scalability of chemical methods by using redox buffers to fine-tune the Fermi level of the film through reversible charge transfer *from solution* (Figure 1). Through the use of a redox buffer, the solution potential can

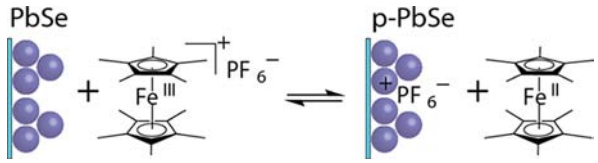

Figure 1. Equilibrium oxidation of a PbSe nanocrystal solid by Fc^{*+} accompanied by infiltration of the PF_6^- counterion into the film.

easily be tuned over a range of at least ±180 mV relative to the standard potential of the reagent, E^0, by varying the concentration ratio of the oxidized and reduced species [see the Supporting Information (SI)]. Because of the wide array of available redox reagents, displaying a range of over 3 V in standard potential,[16] we envisioned that exposing nanocrystal solids to an appropriate redox buffer solution would allow for precise thermodynamic control over the dopant density in the film.

Here we demonstrate the controlled doping of ethanedithiol (EDT)-treated lead selenide (PbSe) nanocrystal solids using the decamethylferrocene/decamethylferrocenium (Fc^*/Fc^{*+}) redox buffer. The carrier concentration, as determined by field-effect transistor (FET) measurements, can be systematically, incrementally, and reversibly modulated by 2 orders of magnitude from its native value using this simple solution-based technique.

To select an energetically optimal redox couple for the p-type doping of PbSe nanocrystal thin films, we determined the energetics of our target nanocrystal substrate using cyclic voltammetry (CV) (Figure 2). Colloidally synthesized PbSe nanocrystals were deposited onto indium tin oxide (ITO)-coated glass pieces by sequential dip-coating and treated with EDT to effect ligand exchange and enhance the film

Received: May 31, 2012
Published: July 20, 2012

   dx.doi.org/10.1021/ja305293e | J. Am. Chem. Soc. 2012, 134, 13200−13203

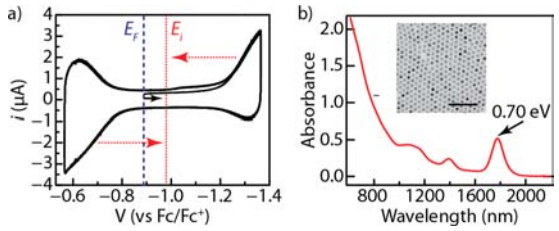

Figure 2. (a) Low-temperature (−37 °C) cyclic voltammogram of an EDT-treated PbSe nanocrystal solid cast onto an ITO working electrode recorded in acetonitrile containing 0.1 M Bu_4NPF_6. The scan was initiated from the open-circuit potential, E_f (blue dashed vertical line), in the negative direction (black arrow) at 200 mV/s. Dotted red arrows serve as guides to the eye indicating the potential E_i (red dotted vertical line) equidistant from the rising anodic and cathodic waves, as calculated in Figure S4. (b) Optical absorbance spectrum of PbSe nanocrystals dispersed in carbon tetrachloride exhibiting a first exciton feature at 0.70 eV (1777 nm). Inset: Transmission electron microscopy (TEM) image of PbSe nanocrystals. The scale bar corresponds to 50 nm.

conductivity.[10] A low temperature (−37 °C) CV of the PbSe nanocrystal-coated ITO electrodes is shown in Figure 2a. In the negative scan starting from the open-circuit potential, a broad quasireversible cathodic wave was observed beginning at −1.2 V (vs Fc/Fc^+) and a broad quasireversible anodic wave was observed beginning at −0.8 V in the return scan. Cycling the electrode over this potential range multiple times (five cycles are shown in Figure 2a) did not cause a significant decrease in the current response for either the cathodic or anodic wave. Additionally, scans taken with a switching potential prior to the cathodic feature also exhibited the anodic wave at −0.8 V (Figure S1 in the SI). Together these observations indicate that the anodic and cathodic waves are not dependent on each other and that the Faradaic current is representative of charge injection rather than parasitic decomposition reactions. These observations are consistent with prior low-temperature CV studies[12−14] and contrast with the irreversible waves observed[17,18] at room temperature. At −37 °C, trapping and decomposition reactions are suppressed, so the potentials of cathodic and anodic charge injection closely approximate the thermodynamic potentials of the electron acceptor and donor states in the film, respectively. Indeed, the ∼0.6 V separation between the cathodic and anodic features is comparable to the energy of the first exciton feature (1777 nm, 0.7 eV; Figure 2b) of the 6.5 ± 0.3 nm PbSe nanocrystals from which the film was cast (Figures S2 and S3). Using the average of the potentials at which the same current was observed for electron and hole injection into the film (Figure 2a and Figure S4), we estimate a midpoint potential of −0.98 ± 0.01 V, corresponding to the Fermi level expected for an intrinsically doped (E_i) nanocrystal film. Importantly, this value is more negative than the open-circuit potential of the native film (−0.89 V; Figure 2a, blue dashed vertical line), indicating that the as-prepared nanocrystal solid is slightly p-type. We note that the estimation of E_i is crude because the cathodic wave is less reversible than the anodic wave.[19] Nevertheless, the p-type nature implied by the CV data is in line with electrical measurements of EDT-treated PbSe nanocrystal solids (see below).[20]

Using the electrochemical information obtained from low-temperature CV, we constructed the energy level diagram shown in Figure 3. The optical band gap of the colloidal PbSe nanocrystals was centered on an absolute energy scale relative

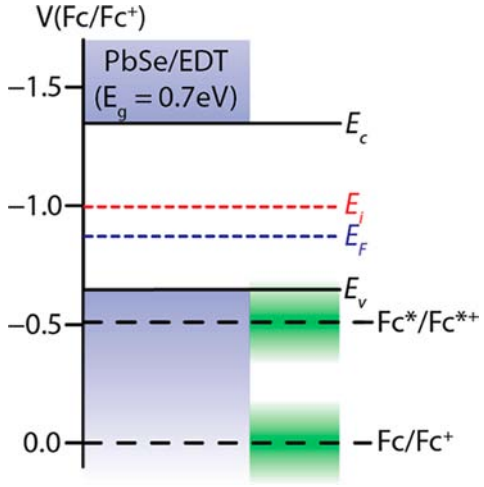

Figure 3. Energy level diagram of an EDT-treated PbSe nanocrystal depicting the conduction band (E_c), the valence band (E_v), the Fermi level of an intrinsically doped film (E_i), the native Fermi level of the as-prepared PbSe film (E_f), and the standard redox potentials of the Fc*/Fc*+ and Fc/Fc^+ redox couples. The shaded green bands indicate the range of solution potentials easily accessible using Fc*/Fc*+ and Fc/Fc^+ redox buffers as given by the Nernst equation.

to the ferrocene/ferrocenium (Fc/Fc^+) redox couple using the E_i value determined from CV. Whereas Fc^+ is too oxidizing to effect controlled doping of this particular PbSe film (see below), the reduction potential of Fc*+ is 0.51 V more negative, making it an ideal candidate for p-type doping. Thus, we examined the electronic effects of exposing PbSe films to Fc*/Fc*+ redox buffers.

Dopant density changes in the nanocrystal solid were extracted from FET measurements. Figure 4a shows that the source−drain characteristics of a freshly fabricated EDT-treated PbSe nanoparticle transistor exhibited ambipolar behavior, consistent with previous results for thiol-capped lead chalcogenide nanoparticles.[5,8] The source−drain current increased and saturated for both positive and negative values

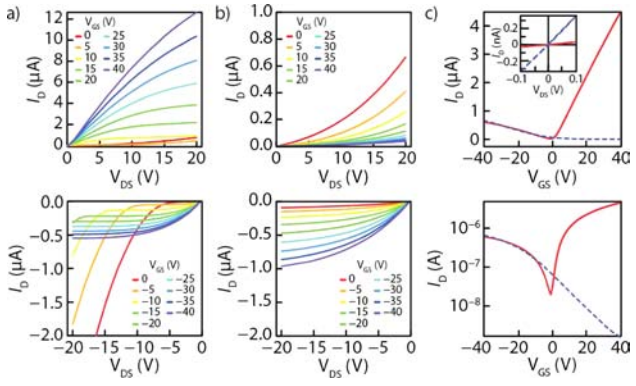

Figure 4. Drain current (I_D) as a function of drain−source voltage (V_{DS}) at a variety of gate−source voltages (V_{GS}) for (a) a native PbSe nanocrystal film and (b) a PbSe nanocrystal film exposed to a 5 mM solution of 1:10 Fc*+:Fc* in acetonitrile. (c) I_D as a function of V_{GS} at V_{DS} = 5 V for a native PbSe nanocrystal film (red solid curve) and the film after doping in a 5 mM solution of 1:10 Fc*+:Fc* in acetonitrile (blue dashed curve). Data are shown on (top) linear and (bottom) logarithmic current axes. Inset: Low-field conductivity (I_D vs V_{DS}) of doped (blue dashed curve) and native (red solid curve) PbSe nanocrystal films held at V_{GS} = 0 V.

dx.doi.org/10.1021/ja305293e | J. Am. Chem. Soc. 2012, 134, 13200−13203

of the gate voltage, indicating injection of both electrons and holes, respectively. The ambipolar nature of the FET was also evidenced by the distinctive takeoff of current in the negative sweep direction as a result of carrier recombination.[21]

Figure 4b shows the source−drain characteristics for the same transistor after it was soaked in a 5 mM solution of 1:10 Fc^{*+}:Fc* in acetonitrile and then washed in pure acetonitrile. Here the device functioned as a unipolar transistor, depleting holes and showing reduced conductivity for positive gate voltages as opposed to accumulating electrons and showing increasing conductivity. The suppression of electron injection was also apparent in the disappearance of the takeoff feature in the negative sweeps. This change in gating behavior can be attributed to a shift in the Fermi level of the channel, as a more positive gate voltage was required for removal of the introduced holes before electrons could be injected.[22]

This shift due to doping is clearly displayed in the transfer plots shown in Figure 4c. Upon doping, electron injection was suppressed ($V_{GS} > 0$), and the transistors shifted from exhibiting ambipolar to unipolar injection. The mobilities for electrons and holes in the untreated films were 0.07 and 0.01 $cm^2\ V^{-1}\ s^{-1}$, respectively. Upon doping, only the hole mobility was measurable, and it was found to decrease slightly to 0.007 $cm^2\ V^{-1}\ s^{-1}$. While the mobility decreased with doping, the small-field conductivity (σ) of the film (Figure 4c inset) rose from 1.4×10^{-6} to 1.5×10^{-5} S cm^{-1}. Following the Ohmic definition of the channel conductivity,[23] $\sigma = n_h e \mu$, where n_h is the density of hole majority carriers (cm^{-3}), e is the charge of an electron, and μ is the linear field-effect mobility, the carrier concentration of the film rose from 5×10^{14} to 1.4×10^{16} cm^{-3} upon doping as a result of both a decrease in the mobility and an increase in the conductance. Notably, none of these changes were observed for films soaked only in pure acetonitrile, electrolyte (Bu_4NPF_6) in acetonitrile, or acetonitrile solutions containing only Fc*.

We investigated the dependence of doping on the redox potential of the solution by varying the Fc^{*+}:Fc* ratio of the redox buffer. Figure 5 shows the effect on the FET performance of varying the [Ox]:[Red] ratio over 3 orders of magnitude, covering a redox potential range ~180 mV to ~360 mV positive of the open-circuit potential of the untreated films. Over this range, the conductivity exhibited a steady monotonic increase by a factor of ~20, while the linear field-effect mobility decreased by a similar magnitude, leading to carrier concentrations extracted from Ohm's law displaying an increase of 2 orders of magnitude. The precise origin of the decrease in field effect mobility is unclear at present, but it may be due to increasing energetic site disorder[5] or partial screening of the gate field due to counterion mobility within the film.[24] Nevertheless, the electronic data indicates that increasing the redox potential of the buffer solution incrementally modulates the dopant density in the film.

Importantly, the increases in carrier concentration did not correspond precisely to that expected on the basis of the change in the solution potential: a ~360 mV shift in solution potential resulted in a shift of only ~120 meV in the Fermi level of the film (2 orders of magnitude increase in carrier concentration). In analogy to what has been documented for semiconductor/solution junctions,[25,26] we suspect that the high population of localized surface states in the nanocrystal film[19] causes an increased potential drop across the Helmholtz double layer and partially pins the Fermi level of the nanocrystal solid, thereby preventing a straightforward correspondence between the

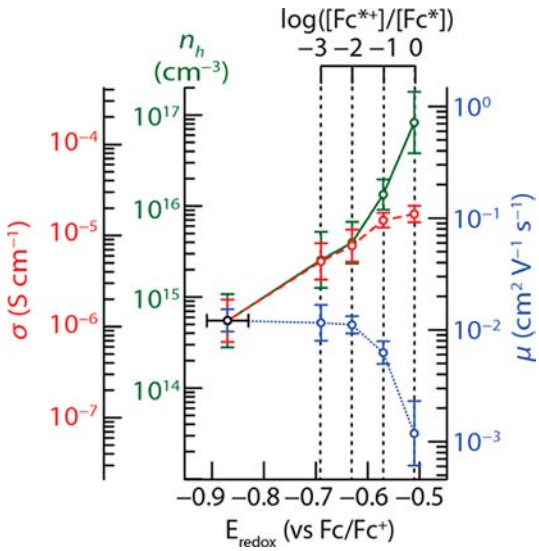

Figure 5. Small-field conductivity σ (red dashed curve), linear field-effect mobility μ (blue dotted curve), and hole majority carrier density n_h (green solid curve) of PbSe nanocrystal solid films as a function of the potential of the Fc^*/Fc^{*+} doping solution. The potential of the native film (first point at the left), taken as the room-temperature open-circuit potential measured in acetonitrile containing 0.1 M Bu_4NPF_6, is the average of five measurements on independently prepared films cast onto ITO-coated electrodes. Error bars in the electronic properties represent the geometric standard deviations about the geometric mean of at least nine devices on three independently prepared and doped nanocrystal films.

solution potential and the carrier concentration in the film. While charge trapping may lead to higher counterion concentrations than free carrier concentrations, X-ray photoelectron spectroscopy (XPS) failed to detect PF_6^- in the treated film (Figure S5), suggesting an upper limit of ~10^{19} cm^{-3} or ~3 per nanoparticle (see the SI for the detailed calculation). Thus, we expect that films possessing lower surface trap densities will be amenable to more efficient and stable doping using redox buffers.

To ensure that the doping occurred under thermodynamic control, we examined the time course and reversibility of the charge transfer reaction. Figure 6 illustrates changes in the dopant density (n_h) of a PbSe nanocrystal FET as a function of soaking time in the presence of a series of buffers with different Fc*+/Fc* ratios (see Figure S6 for raw σ and μ values). The first point was measured from untreated films. which then became lightly doped to a steady-state value upon soaking in a 1:1000 Fc^{*+}:Fc* buffer. In the middle frame, the transistors were soaked in more oxidative buffers (1:100 and 1:10 for open squares and solid circles, respectively) and reached new steady-state levels of doping corresponding to the increased oxidizing powers of the buffers. In the last frame, the transistors were both soaked again in the original buffer (1:1000) and eventually returned to their earlier levels of doping. While the frustrated kinetics of diffusion in a microporous network[27] led to a differing time for each system to reach equilibrium, the time invariance following equilibration and the reversibility of the attendant doping level establish that doping occurred under thermodynamic control. As expected, a time-invariant equilibrium doping level was not obtained when PbSe films were exposed to a solution potential well beyond the valence band edge. A monotonic increase in dopant concentration with time, indicative of kinetically limited doping, occurred when PbSe

dx.doi.org/10.1021/ja305293e | J. Am. Chem. Soc. 2012, 134, 13200−13203

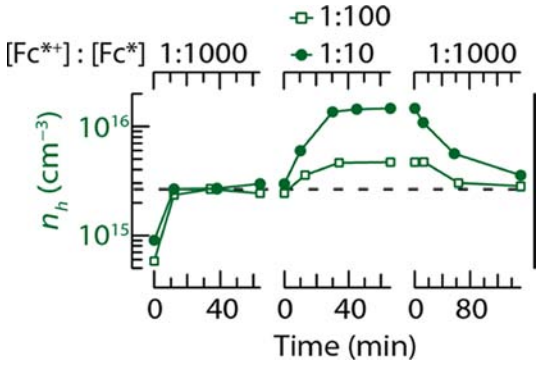

Figure 6. Hole majority carrier densities (n_h) for two PbSe nanocrystal solid films as functions of the time duration of exposure to Fc*/Fc*$^+$ doping solutions. The initial points represent untreated films. Both films were exposed to a 5 mM 1:1000 Fc*$^+$:Fc* doping solution in acetonitrile for the first and last time series, whereas in between one was exposed to a 5 mM 1:10 doping solution (●) and the other to a 5 mM 1:100 doping solution (□).

films were exposed to highly oxidixing Fc$^+$ solutions (Figure S7).

The equilibrium between the nanoparticle film and the redox buffer solution is metastable, as it exists under a chemically applied electrochemical potential while soaking. When the film is removed from the solution, it settles into a new metastable equilibrium in which charge has been injected and "frozen in", even though the film no longer experiences a chemically imposed potential. Figure S8 shows that the extracted carrier concentration drops over this initial period but then levels out to a steady value. Thus, despite some initial reconfiguration, a large fraction of free carriers remains, leaving films whose doping concentrations are controllable and stable.

In conclusion, we have demonstrated that PbSe nanocrystal solids can be controllably subjected to p-type doping under thermodynamic control by exposure to Fc*/Fc*$^+$ redox buffers. Studies are underway to extend this doping strategy to n-type doping as well as to other materials systems.

■ ASSOCIATED CONTENT

Ⓢ Supporting Information

Full experimental details, additional CVs, TEM images, sizing statistics, XPS spectra, Fc$^+$ doping results, and time dependence of carrier concentrations. This material is available free of charge via the Internet at http://pubs.acs.org.

■ AUTHOR INFORMATION

Corresponding Author

apalivisatos@lbl.gov

Author Contributions

‖J.H.E. and Y.S. contributed equally.

Notes

The authors declare no competing financial interest.

■ ACKNOWLEDGMENTS

We are grateful to W. E. Geiger, M. L. Tang, and M. Wu for helpful discussions. We thank J. M. Luther for the nanoparticle samples, J. Niskala for the patterned silicon substrates, and B. Beberwyck for assistance with TEM. The work by J.H.E. was supported by Self-Assembly of Organic/Inorganic Nanocomposite Materials (Grant DE-AC02-05CH11231 to A.P.A.). Y.S. acknowledges the Miller Institute for Basic Research in Science for a postdoctoral fellowship.

■ REFERENCES

(1) Talapin, D. V.; Lee, J.-S.; Kovalenko, M. V.; Shevchenko, E. V. *Chem. Rev.* **2010**, *110*, 389.
(2) Semonin, O. E.; Luther, J. M.; Choi, S.; Chen, H.-Y.; Gao, J.; Nozik, A. J.; Beard, M. C. *Science* **2011**, *334*, 1530.
(3) Tang, J.; Kemp, K. W.; Hoogland, S.; Jeong, K. S.; Liu, H.; Levina, L.; Furukawa, M.; Wang, X.; Debnath, R.; Cha, D.; Chou, K. W.; Fischer, A.; Amassian, A.; Asbury, J. B.; Sargent, E. H. *Nat. Mater.* **2011**, *10*, 765.
(4) Dai, Q.; Wang, Y.; Li, X.; Zhang, Y.; Pellegrino, D. J.; Zhao, M.; Zou, B.; Seo, J.; Wang, Y.; Yu, W. W. *ACS Nano* **2009**, *3*, 1518.
(5) Liu, Y.; Gibbs, M.; Puthussery, J.; Gaik, S.; Ihly, R.; Hillhouse, H. W.; Law, M. *Nano Lett.* **2010**, *10*, 1960.
(6) Shim, M.; Guyot-Sionnest, P. *Nature* **2000**, *407*, 981.
(7) Talapin, D.; Murray, C. *Science* **2005**, *310*, 86.
(8) Leschkies, K. S.; Kang, M. S.; Aydil, E. S.; Norris, D. J. *J. Phys. Chem. C* **2010**, *114*, 9988.
(9) Mocatta, D.; Cohen, G.; Schattner, J.; Millo, O.; Rabani, E.; Banin, U. *Science* **2011**, *332*, 77.
(10) Luther, J. M.; Law, M.; Song, Q.; Perkins, C. L.; Beard, M. C.; Nozik, A. J. *ACS Nano* **2008**, *2*, 271.
(11) Kutana, A.; Erwin, S. C. *Phys. Rev. B* **2011**, *83*, No. 235419.
(12) Yu, D.; Wang, C.; Guyot-Sionnest, P. *Science* **2003**, *300*, 1277.
(13) Liu, H.; Keuleyan, S.; Guyot-Sionnest, P. *J. Phys. Chem. C* **2012**, *116*, 1344.
(14) Houtepen, A. J.; Kockmann, D.; Vanmaekelbergh, D. *Nano Lett.* **2008**, *8*, 3516.
(15) Fabregat-Santiago, F.; Mora-Seró, I.; Garcia-Belmonte, G.; Bisquert, J. *J. Phys. Chem. B* **2003**, *107*, 758.
(16) Connelly, N. G.; Geiger, W. E. *Chem. Rev.* **1996**, *96*, 877.
(17) Choi, J. J.; Lim, Y.-F.; Santiago-Berrios, M. B.; Oh, M.; Hyun, B.-R.; Sun, L.; Bartnik, A. C.; Goedhart, A.; Malliaras, G. G.; Abruña, H. D.; Wise, F. W.; Hanrath, T. *Nano Lett.* **2009**, *9*, 3749.
(18) Jiang, X.; Schaller, R. D.; Lee, S. B.; Pietryga, J. M.; Klimov, V. I.; Zakhidov, A. A. *J. Mater. Res.* **2007**, *22*, 2204.
(19) This is in accord with the observation of significant electron trapping in PbSe films. See: Konstantatos, G.; Levina, L.; Fischer, A.; Sargent, E. H. *Nano Lett.* **2008**, *8*, 1446.
(20) Wang, R. Y.; Feser, J. P.; Lee, J.-S.; Talapin, D. V.; Segalman, R.; Majumdar, A. *Nano Lett.* **2008**, *8*, 2283.
(21) Zaumseil, J.; Friend, R.; Sirringhaus, H. *Nat. Mater.* **2006**, *5*, 69.
(22) Sze, S. M.; Ng, K. K. *Physics of Semiconductor Devices*, 3rd ed.; Wiley: Hoboken, NJ, 2007.
(23) Klem, E. J. D.; Shukla, H.; Hinds, S.; MacNeil, D. D.; Levina, L.; Sargent, E. H. *Appl. Phys. Lett.* **2008**, *92*, No. 212105.
(24) Chua, L.; Zaumseil, J.; Chang, J.; Ou, E.; Ho, P.; Sirringhaus, H.; Friend, R. *Nature* **2005**, *434*, 194.
(25) Bard, A. J.; Bocarsly, A. B.; Fan, F. R. F.; Walton, E. G.; Wrighton, M. S. *J. Am. Chem. Soc.* **1980**, *102*, 3671.
(26) Lewerenz, H. J. *J. Electroanal. Chem.* **1993**, *356*, 121.
(27) Havlin, S.; Benavraham, D. *Adv. Phys.* **1987**, *36*, 695.